Clean Energy Science and Technology 2024, 2(2), 138
https://doi.org/10.18686/cest.v2i2.138

Article

High-performance proton exchange membrane employing water-insoluble hybrid formed by chemically bonding phosphotungstic acid with polydopamine

Zhongrui Lu, Xiancan Yuan, Xiaoyang Jia, Jun Lin*, Shaojian He*

State Key Laboratory of Alternate Electrical Power System with Renewable Energy Sources, North China Electric Power University, Beijing 102206, China

*** Corresponding authors:** Jun Lin, jun.lin@ncepu.edu.cn; Shaojian He, heshaojian@ncepu.edu.cn

CITATION

Lu Z, Yuan X, Jia X, et al. High-performance proton exchange membrane employing water-insoluble hybrid formed by chemically bonding phosphotungstic acid with polydopamine. Clean Energy Science and Technology. 2024; 2(2): 138. https://doi.org/10.18686/cest.v2i2.138

ARTICLE INFO

Received: 4 March 2024
Accepted: 26 April 2024
Available online: 7 May 2024

Abstract: Heteropolyacids can retain water in a proton exchange membrane to increase proton conductivity at high temperatures and low humidity; however, their high solubility in water leads to leaching, which limits their further application. Herein, we used phosphotungstic acid (HPW) and polydopamine (PDA) particles to prepare a water-insoluble PDA/HPW hybrid (PDW) via hydrothermal reaction. The amino groups of PDA in PDW chemically bonded to HPW and acted as an anchor for HPW. The proton conductivity of the sulfonated poly(ether ether ketone) (SPEEK) composite membrane containing 15wt% PDW (SPEEK/PDW-15) in liquid water was 0.052 $S \cdot cm^{-1}$ at 25 ℃, which was 63% higher than that of the SPEEK control membrane (0.032 $S \cdot cm^{-1}$). The SPEEK/PDW-15 composite membrane also showed stable proton conductivity during 80 days of testing while immersed in water.

Keywords: proton exchange membrane for fuel cell; sulfonated poly(ether ether ketone); phosphotungstic acid; polydopamine; hydrothermal

1. Introduction

Global climate change has become a major environmental threat and challenge for all kinds of creatures on the earth, including humans [1–3]. Various strategies have been employed to reduce fossil fuel over-consumption and environmental pollution, which are responsible for global climate change [4–6]. The utilization of clean energy is one of the most important strategies. Hydrogen energy is a globally recognized ideal solution for clean energy, and the fuel cell is an electrochemical device that directly converts hydrogen energy into electrical energy [7]. Proton-exchange-membrane fuel cells (PEMFCs) have become the focus of research globally due to their advantages of high theoretical efficiency, high power density, simple operation, and pollution-free emission [8–12]. Theoretically, PEMFCs present a higher energy conversion efficiency when operating at higher temperatures. However, as the core component of PEMFCs to conduct protons, the proton exchange membrane (PEM) tends to dehydrate at high temperatures and low humidity, which severely reduces its proton conductivity. This phenomenon hinders the further development and commercialization of PEMFCs [13].

Heteropolyacids (HPAs), such as phosphotungstic acid ($H_3PW_{12}O_{40}$, HPW), are widely used to enhance the proton conductivity of PEMs because of their excellent thermal stability and strong acidity, as well as good water retention properties at low humidity [14–17]. However, HPAs in composite membranes are highly water-soluble and can be easily dissolved. It has been reported that the mass loss of HPW reached

93.5 wt% after immersing a 30wt% HPW-doped sulfonated poly(ether ether ketone) (SPEEK) composite membrane in water for 30 days at 80 ℃ [18]. Therefore, it is of great importance to immobilize HPAs in composite membranes to achieve high performance.

Dopamine, the main component of adhesion proteins in mussels, can be oxidized and self-polymerized to form polydopamine (PDA) in weakly alkaline aqueous solutions. PDA can be easily and stably deposited on almost all types of substrates [19–22]. In addition, the chemical structure of PDA contains many functional groups, such as catechols and amines [23–25]. These two characteristics endow PDA the ability to modify a substrate to immobilize HPW in PEMs [17,26–29]. For example, He et al. [30] used PDA-coated halloysite nanotubes (DHNTs) as binding sites to immobilize HPW. The proton conductivity of the nanocomposite membrane loaded with 15wt% DHNTs and 42.9wt% HPW (0.117 $S \cdot cm^{-1}$) increased by 114% compared with that of the SPEEK control membrane. Owing to the acid-base interactions between amino groups in PDA and HPW, only a slight decrease in proton conductivity was found under the long-term water immersion test. Wei et al. [28] incorporated PDA-coated polyimide (PI) into a SPEEK membrane to anchor HPW via acid-base pairs, and the membrane proton conductivity reached a maximum of 0.212 $S \cdot cm^{-1}$ at 60 ℃ and 100% relative humidity (RH). After a six-week test, the loss of proton conductivity was reduced by 51% compared with that of the composite membrane without PDA-coated PI.

Nevertheless, it is difficult to completely solve the leaching problem of soluble proton carriers through electrostatic interactions, and so chemical bonding to anchor HPW has been considered a better option. Zhai et al. [31] synthesized nanohybrids using the imine groups of covalent organic frameworks to react with HPW via a hydrothermal method to immobilize HPW, and they found that no HPW dissolved after immersing nanohybrids in deionized water for three months. Zhang et al. [32] encapsulated HPW in MIL-101(Fe) using a hydrothermal method, which was then doped into a sulfonated poly(arylene ether ketone sulfone) (SPAEKS) matrix. The proton conductivity of the composite membrane reached up to 0.072 $S \cdot cm^{-1}$ (1.8 times that of pure SPAEKS) at 80 ℃ and 100% RH and remained almost unchanged at 30 ℃ for 30 days.

Inspired by the two different strategies mentioned above, we believe that HPW is capable of bonding to amino groups under certain conditions to form a stable structure. Therefore, in this work, we utilized a simple one-step hydrothermal method to synthesize water-insoluble PDA/HPW (PDW) hybrid, where HPW and PDA were bonded together by chemical bonding. PDW can act as the proton conductor in the composite membrane, shortening the distance of proton hopping and effectively increasing the proton conductivity of the composite membrane. The water-insoluble nature of PDW also can ensure the stable proton conductivity of the composite membrane over the course of the 80-day test. In addition, the excellent water retention ability of HPW can endow the composite membrane with good proton conductivity even at low RH. Hence, the structure, morphology, and physicochemical properties of the composite membrane with PDW hybrid were investigated.

2. Experiment

2.1. Materials

Dopamine hydrochloride (98%) and HPW were purchased from Innochem Science & Technology Co. Ltd. (Beijing, China). Sodium hydroxide (NaOH, 99%) and Tris(hydroxymethyl)aminomethane hydrochloride (Tris-HCL, 99%) were bought from Alfa Aesar. Concentrated sulfuric acid (95–98%) and concentrated hydrochloric acid (36–38%) were purchased from China National Medicines Co. Ltd. (Beijing, China). Poly(ether ether ketone) (PEEK) (Victrex 450 PF) was purchased from Victrex (Lancashire, UK). N, N-dimethylacetamide (DMAc), and ethanol were bought from Boenchuangqi Company (Beijing, China).

2.2. Sample preparation

Preparation of PDA: 0.3 g Tris-HCL was added into a mixture of 110 mL deionized (DI) water and 40 mL ethanol. Then the pH of the solution was adjusted to 8.5 using NaOH, followed by the addition of 1.0 g dopamine hydrochloride. After 24 h of stirring, the precipitate was filtered, washed repeatedly for four times with DI water, and then dried in a freeze dryer for 24 h to obtain PDA.

Preparation of PDW hybrid: Following the above-mentioned procedure, dopamine was stirred and polymerized for 24 h, and then 13.6 mL concentrated hydrochloric acid and 5.0 g HPW were added into the suspension in sequence. After being stirred for 1 h, the mixture was subjected to hydrothermal treatment at 150 ℃ for 24 h. The precipitate was repeatedly filtered and washed with DI water at least four times, and then it was dried in a freeze dryer for 24 h. The resulting product was denoted as PDW.

Preparation of SPEEK: First, 15.0 g poly(ether ether ketone) powder was dried in a vacuum oven for 24 h at 80 ℃. After that, the powder was added to 300 mL of concentrated sulfuric acid and stirred intensely at 25 ℃ for 24 h. Thereafter, the obtained solution was slowly poured into an ice-water mixture to solidify and prevent the sulfonation reaction. The flocculated filaments were washed with DI water for several times until the solution reached neutrality. The obtained product was dried at 40 ℃ for 24 h and then dried at 80 ℃ for another 24 h to obtain SPEEK.

Preparation of SPEEK/PDW composite membranes: Certain amounts of PDW and SPEEK (a total of 0.3 g) were added to 5.0 mL DMAc. The suspension was sonicated for 2 h and then stirred for 24 h. After pulling the air out, the suspension was cast into a glass dish and placed in a blast oven at 80 ℃ for 24 h. Subsequently, it was dried in a vacuum oven at 80 ℃ for another 24 h. The membranes were treated with 1M H_2SO_4 and DI water afterward. The resulting membranes were indicated as SPEEK/PDW-*x*, where *x* is the weight percent of PDW.

2.3. Characterizations and measurements

X-ray diffraction (XRD) patterns were obtained using a diffractometer (SmartLab SE, Rigaku) with a Cu-Kα source (λ = 1.54 Å) at a scan rate of $5°\cdot min^{-1}$ and a scan range from 5° to 60°. The structures of the powders were characterized via Fourier transform infrared spectroscopy (FTIR) (Nicolet IS10, Thermo Fisher Scientific) in

the range of 600–2000 cm^{-1}. The powders were observed using a transmission electron microscope (TEM) (JEM-2100Plus, JEOL) at an accelerating voltage of 200 kV. Scanning electron microscopy (SEM) (Quattro S, Thermo Scientific) was used to observe the morphology of the samples at an accelerating voltage of 15 kV, and energy dispersive X-ray spectroscopy (EDS) was used to probe the distribution of the elements in the PDW. X-ray photoelectron spectroscopy (XPS) (K-Alpha, Thermo Scientific) was performed on the powders using an Al-Kα source at a working pressure of about 3×10^{-7} mba. Thermogravimetric analysis (TGA) (TGA 550, TA) was carried out under a nitrogen atmosphere from 30 ℃ to 800 ℃ with a heating rate of 20 ℃ min^{-1}.

The proton exchange membranes were immersed in DI water at room temperature to ensure complete hydration.

The water uptake and swelling ratio of the membranes were determined according to Equation (1) and Equation (2), separately:

$$Water\ uptake\ (\%) = \frac{M_w - M_d}{M_d} \times 100\% \quad (1)$$

$$Swelling\ ratio\ (\%) = \frac{S_w - S_d}{S_d} \times 100\% \quad (2)$$

where M_w is the weight of the wet membrane after the rapid removal of surface moisture, and M_d is the weight of the dried membrane, while S_w and S_d are the areas of the wet and dried membranes, respectively.

The ion exchange capacity (IEC) of the membranes was determined via the acid-base titration method. Typically, a dried membrane sample was immersed in 20 mL NaCl solution (2.00 $mol \cdot L^{-1}$) for 24 h to release H^+ ions and then titrated with a standard NaOH solution (0.01 $mol \cdot L^{-1}$) using phenolphthalein as an indicator. The formula for IEC is as follows:

$$IEC = \frac{(0.0100 \times V_{NaOH})}{M_d} \quad (3)$$

where V_{NaOH} is the volume of the NaOH solution used for titration.

The proton conductivity (σ) of the membranes was tested via an electrochemical workstation (ZENNIUM PRO, Zahner) using the AC impedance technique. A membrane sample was first placed in a four-electrode conductivity clamp (BT110, BekkTech LLC) and then put in liquid DI water or a humidity chamber (YSGDS-50, YISHUO, Shanghai) to reach the desired humidity. Proton conductivity is determined using the following equation:

$$\sigma = \frac{L}{RS} \quad (4)$$

where L is the distance between the two inner electrodes in the conductivity clamp (0.50 cm), S is the cross-sectional area of the membrane sample, and R is membrane resistance.

3. Results and discussion

3.1. Structure and morphology of PDW

To investigate the crystal structure of the hybrid particles, the XRD analysis of HPW, PDA, and PDW was carried out. As shown in **Figure 1(a)**, there was a broad

diffraction peak at 2θ = 24° in the XRD pattern of PDA, which was consistent with those in previous works, attributed to the fact that PDA samples are typically amorphous polymers [33,34]. For HPW, a typical Keggin structure can be observed [35]. After the hydrothermal reaction of HPW with PDA, the XRD curves changed significantly. This phenomenon was due to the strong interaction between HPW and PDA during the hydrothermal process, resulting in a change in the crystal structure of PDW compared with that of HPW. Notably, the physical mixing of PDA and HPW at a mass ratio of 1:5, noted as PDA/HPW-mixed in **Figure 1(a)**, was analyzed and compared. The XRD pattern of PDA/HPW-mixed was the same as that of HPW. The physical cladding of PDA did not change the crystal structure of HPW. This phenomenon further confirmed that the PDW was not a mechanical mixture of HPW and PDA.

The structures of HPW, PDA, and PDW were further investigated using FTIR analysis. As shown in **Figure 1(b)**, four characteristic peaks of HPW can be observed. The peak at 1076 cm^{-1} corresponded to the stretching vibrations of P-O_a bonds in the PO_4 unit. Moreover, the peaks at 956 cm^{-1}, 880 cm^{-1}, and 786 cm^{-1} were associated with W=O_d, W-O_b-W, and W-O_c-W bonds of Keggin units, respectively [36,37]. For PDA, the peaks at 1591 cm^{-1}, 1508 cm^{-1}, and 1280 cm^{-1} belonged to C=C stretching vibrations, N-H shear vibrations, and C-N shear vibrations, respectively [38,39]. As for PDW, the characteristic peaks of PDA at 1200–1600 cm^{-1} still existed and the characteristic peaks of the Keggin structure from HPW can also be seen clearly. However, the peaks of the Keggin structure in PDW showed a slight offset compared with those of HPW. This suggested that there was an interaction between HPW and PDA during the hydrothermal process, which was also confirmed by the XRD characterization.

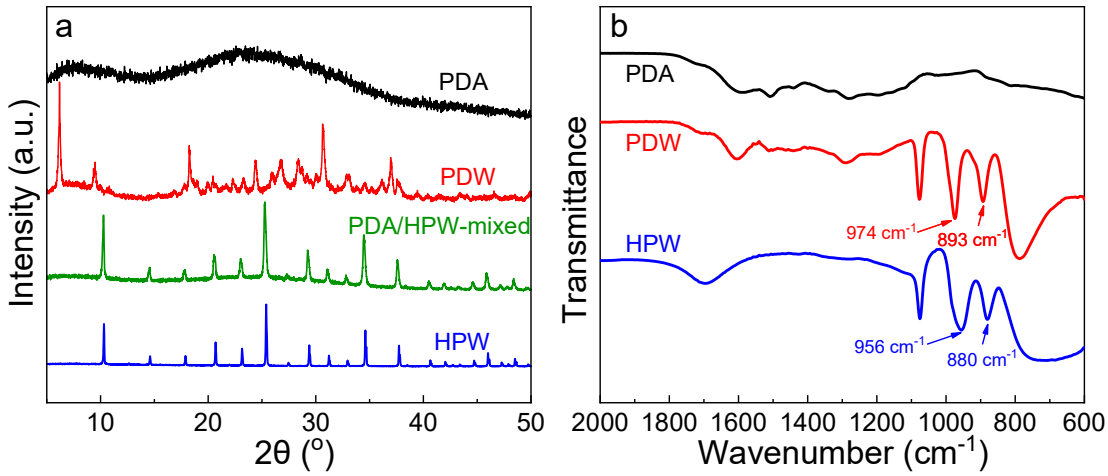

Figure 1. (a) XRD patterns of PDA, PDW, HPW, and PDA/HPW-mixed. **(b)** FTIR spectra of PDA, PDW, and HPW.

XPS analysis was deployed to probe the chemical states of the elements in PDA, HPW, and PDW. From **Figure 2(a)**, the peaks in the C1s spectrum of PDW remained unchanged compared with those of PDA, indicating that the chemical environment of C atoms did not change after the reaction of PDA with HPW. In the N1s spectra shown in **Figure 2(b)**, the N1s peaks of PDA at 399.8 eV and 401.7 eV were attributed to -NH- and -NH_2, respectively. The N1s peaks of PDW shifted toward a higher binding

energy due to the interaction between HPW and PDA. The significant enhancement of the peak at 402.1 eV for PDW can be attributed to the formation of -NH^{3+} [40]. In **Figure 2(c)**, the O1s peak corresponding to C-O in PDA shifted from 532.1 eV to 531.3 eV in PDW. This implied that C-O-W covalent bonds may have been formed after the hydrothermal reaction [41]. In **Figure 2(d)**, the W4f characteristic peaks of HPW at 37.9 eV and 35.8 eV shifted to 38.5 eV and 36.4 eV in PDW, respectively. This suggested a decrease in the electron density of HPW in PDW and the presence of an electron transfer between HPW and PDA [31]. Consequently, the creation of the chemical bonding between PDA and HPW in PDW was further confirmed by the XPS results.

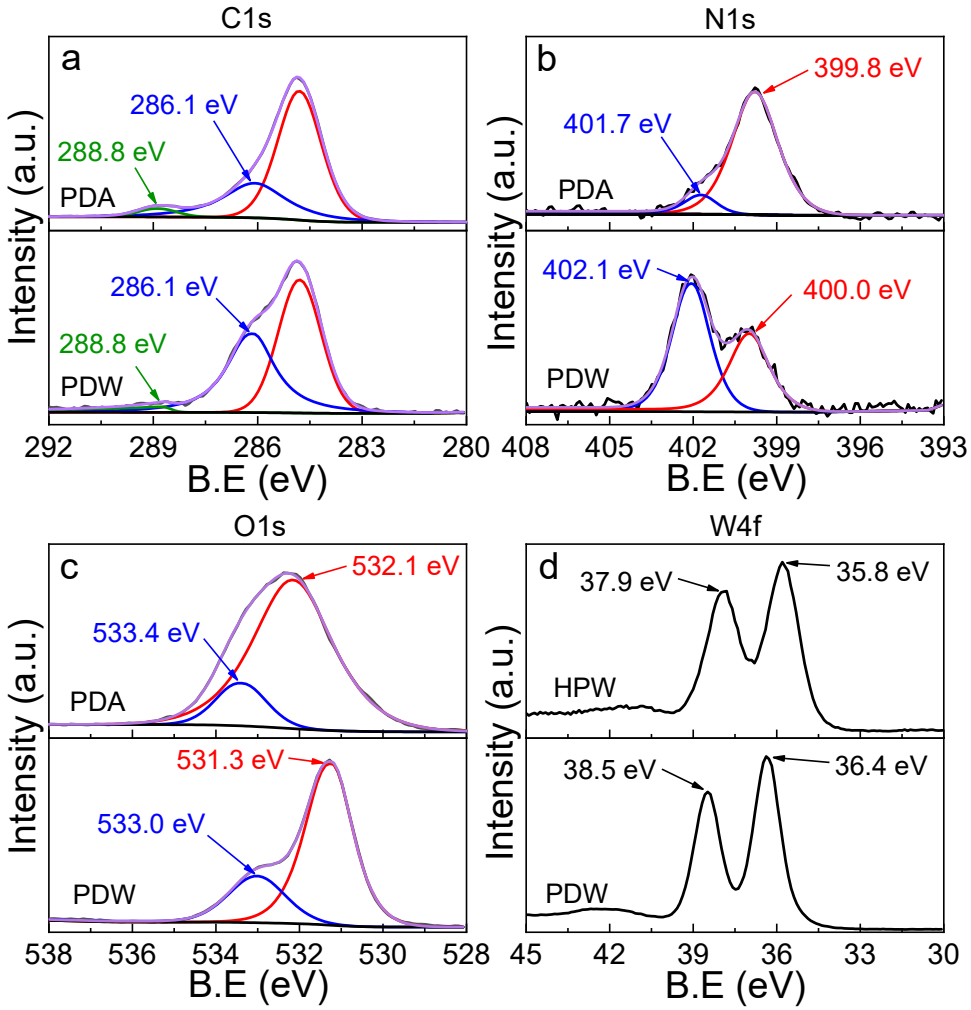

Figure 2. XPS spectra of PDA and PDW: **(a)** C1s; **(b)** N1s; **(c)** O1s; XPS spectra of HPW and PDW: **(d)** W4f.

The thermal stability of PDA, HPW, and PDW was investigated using thermogravimetric analysis (TGA). As shown in **Figure 3**, there were three main stages of the thermal decomposition of PDA. The weight loss below 120 ℃ was mainly due to the evaporation of water in PDA. The second stage of weight loss was related to the decomposition of the catechol fraction. The weight loss above 350 ℃ was mainly attributed to the degradation of the PDA backbone, which is in agreement with that in a previous work [42]. For HPW, the two weight loss stages below 200 ℃ were mainly due to the evaporation of physically adsorbed water and water of

crystallization. Apart from that, there was almost no further weight loss for HPW at 200 ℃–800 ℃. As for PDW, it had better thermal stability below 450 ℃ compared with those of PDA and HPW. By having approximately 86% of the mass of PDW remaining at 800 ℃, the weight ratio of HPW to PDA in PDW can be calculated to be ~5:1.

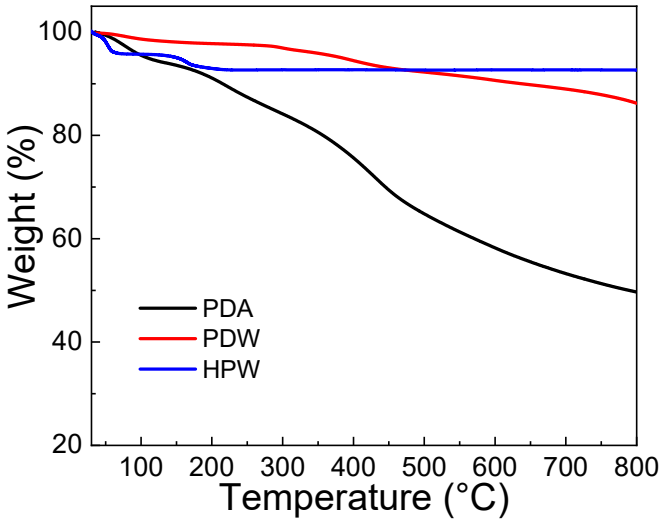

Figure 3. TGA curves of PDW, HPW, and PDA.

The morphologies of PDA and PDW were observed using SEM and TEM. As shown in **Figure 4(a)**, PDA particles displayed a typical spherical structure with a uniform size of about 200 nm, which was also confirmed in **Figure 4(d)**. PDW particles in **Figure 4(b)** exhibited a similar spherical structure to that of the PDA. Nevertheless, the shapes, sizes, and edges of PDW particles were no longer as uniform as those of PDA after the hydrothermal reaction. The presence of HPW in PDW can be confirmed by the EDS plot in **Figure 4(c)**. From TEM analysis, there was no lattice structure in amorphous PDA. However, there were various lattice fringes with different lattice spacings in PDW, as shown in **Figure 4(f)**, which corresponded to crystal planes. This was consistent with the XRD result shown in **Figure 1(a)**.

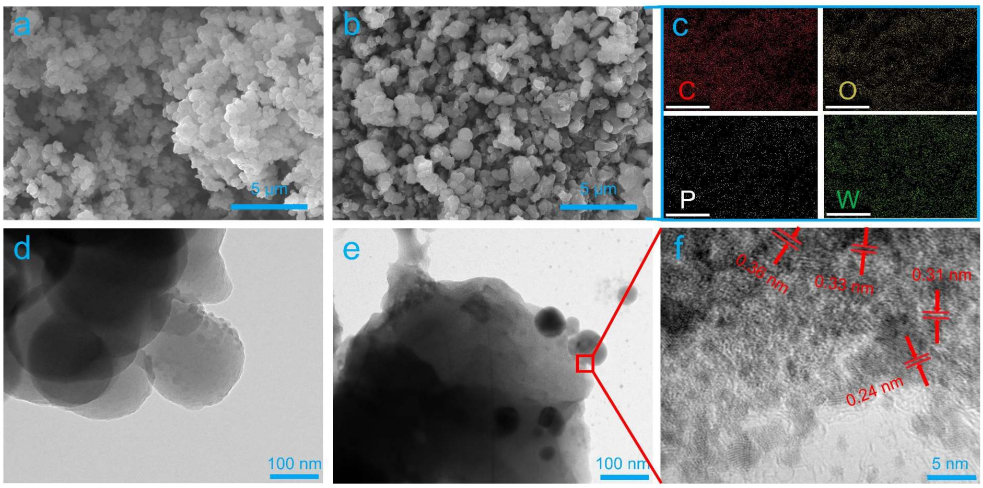

Figure 4. (a) SEM image of PDA. **(b)** SEM image of PDW. **(c)** EDS maps of PDW. **(d)** TEM image of PDA. **(e)** TEM image of PDW in low resolution. **(f)** TEM image of PDW in high resolution.

3.2. Structures and properties of composite membranes

The distribution of PDW in the SPEEK matrix and the microstructures of the membranes were observed via SEM. **Figure 5** shows the cross-sectional images of SPEEK and SPEEK/PDW-*x* membranes. The SPEEK control membrane exhibited a dense morphology. PDW was well dispersed in the composite membranes when the content of PDW was less than 15 wt%. In addition, the fracture surfaces of the SPEEK/PDW composite membranes were all very homogeneous with no voids or defects, as observed in **Figure 5(b–d)**, which suggested that the PDW fillers had good compatibility with the SPEEK matrix. This phenomenon may be mainly due to the strong electrostatic interactions between the hydrophilic groups in PDW and SPEEK. Nevertheless, when the content of PDW reached 20 wt%, defects, such as the aggregation of PDW hybrid and holes, can be observed.

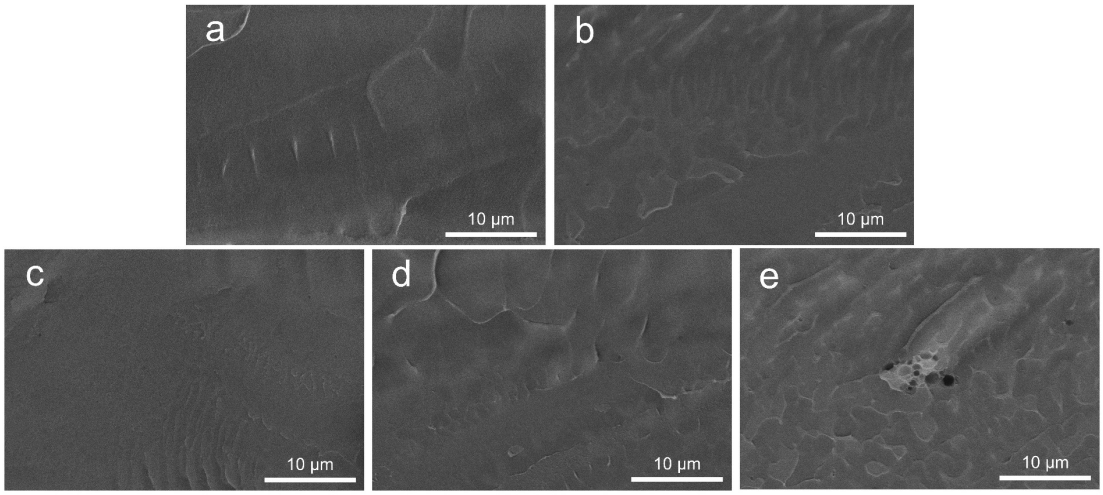

Figure 5. Cross-sectional SEM images of membranes: **(a)** SPEEK control, **(b)** SPEEK/PDW-5, **(c)** SPEEK/PDW-10, **(d)** SPEEK/PDW-15, and **(e)** SPEEK/PDW-20.

As shown in **Figure 6(a)**, the proton conductivity of the SPEEK/PDW composite membrane increased significantly with the increase in filler loading. The SPEEK/PDW-15 membrane exhibited proton conductivity of 0.052 $S \cdot cm^{-1}$, which was 63% higher than that of the SPEEK control membrane (0.032 $S \cdot cm^{-1}$). For comparison, the proton conductivity of the SPEEK/PDA composite membrane filled with 3wt% PDA was tested, which showed a slight decrease to 0.029 $S \cdot cm^{-1}$ (blue dashed line in **Figure 6(a)**) compared with that of the SPEEK control membrane. This indicated that PDA itself was unfavorable for proton transport in composite membranes. Therefore, the significant enhancement of proton conductivity in the SPEEK/PDW composite membranes should be due to the super-strong acidity of HPW. However, when the content of PDW increased to 20 wt%, the proton conductivity of the composite membrane decreased, mainly due to filler aggregation and defects. The comparison of the proton conductivity and promotion ratio (relative to the SPEEK control membrane) between the SPEEK/PDW-15 membrane and other membranes developed in previous works is shown in **Table 1**.

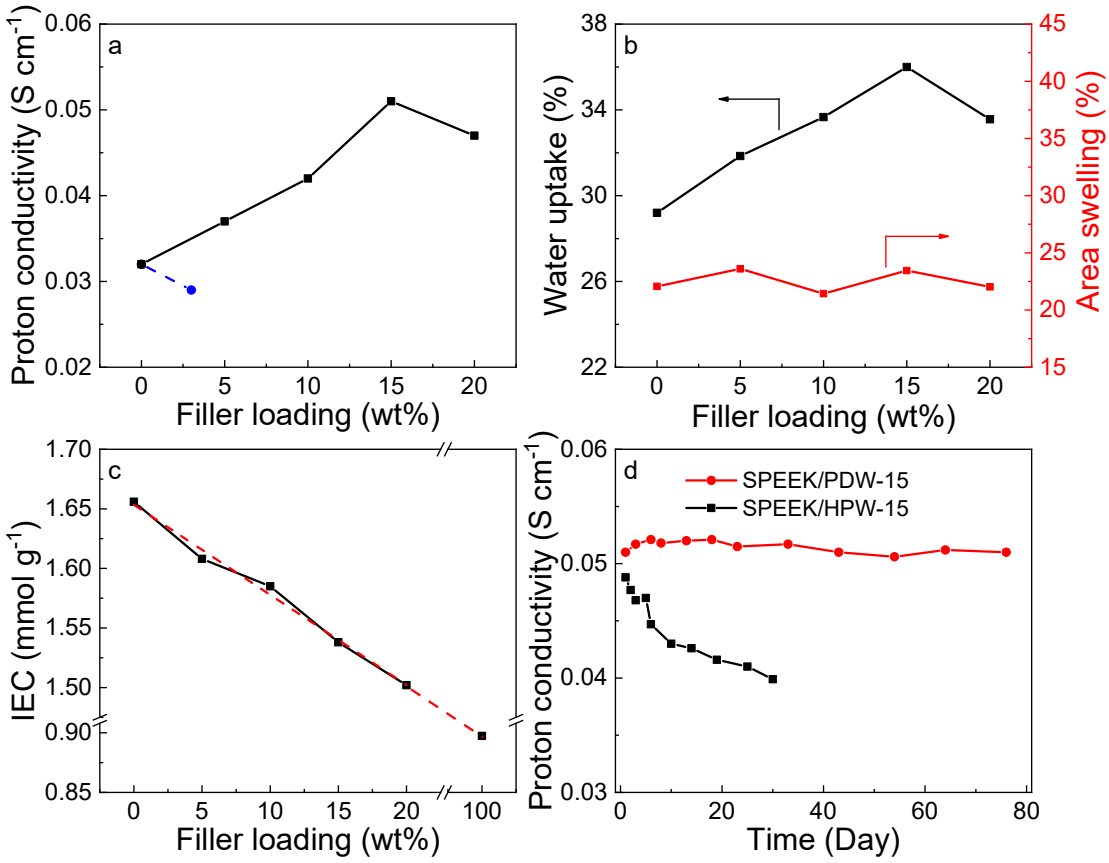

Figure 6. (a) Proton conductivity, **(b)** water uptake and area swelling, and **(c)** IEC of SPEEK control and SPEEK/PDW composite membranes at 25 ℃. **(d)** Proton conductivity of SPEEK/PDW-15 composite membrane at various times during water immersion test at 25 ℃.

Table 1. Comparison between SPEEK/PDW-15 and similar membranes from other studies.

Membrane	Temperature (℃)	Proton conductivity (S·cm^{-1})	Promotion ratio (%)	Ref.
SPEEK/PDW-15	25	0.052	62	This work
S/DCNTs-HPW-1	25	0.027	44	[27]
SPEEK/HPW@MIL-2	20	0.048	26	[43]
SPEEK/EGO-1.5	20	0.034	11	[44]
IL@MIL-125-NH_2/SPEEK-5	25	0.016	60	[45]
SPEEK/ATP-IL-5%	25	0.050	39	[46]
SPEEK/MoS_2@CNTs-1	20	0.042	55	[47]
SPS-3	30	0.038	36	[48]
1.3%NU6@PPNF-SPEEK	60	0.132	25	[49]

Figure 6(b) demonstrates the water uptake and area swelling of the SPEEK control and SPEEK/PDW composite membranes in liquid water as a function of filler content. The water uptake of the composite membrane showed an increasing and then decreasing trend with the increase in PDW loading. The increase in water uptake was attributed to the stronger water absorption ability of PDW with hydrophilic groups, such as phosphotungstate and -NH_2. The water uptake of the composite membrane decreased when the filler content exceeded 15 wt%. This may be related to the aggregation of PDW, as shown in the SEM images, which resulted in interfacial

defects between the SPEEK matrix and the PDW fillers. In contrast, there was very little change in the area swelling of the composite membranes compared with that of the SPEEK control membrane. This phenomenon is mainly due to the strong acid-base pair interaction between PDW and SPEEK controlling the degree of swelling of the membranes upon water uptake. The relatively low swelling of the membranes can improve the stability and durability of membrane electrode assemblies, which is favorable for their application in PEMFCs.

As shown in **Figure 6(c)**, the IEC of the SPEEK/PDW composite membrane decreases almost linearly with the increase in PDW loading. This may be due to the reaction between HPW and PDA, which led to a decrease in the IEC of PDW from HPW (1.04 $mmol \cdot g^{-1}$). Therefore, the IEC of PDW was lower than that of the SPEEK control membrane (1.66 $mmol \cdot g^{-1}$). Notably, a linear extrapolation of the IEC curve to a filler content of 100 wt% (red dashed line in **Figure 6(c)**) yielded an IEC of 0.9 $mmol \cdot g^{-1}$, which was consistent with our reasoning.

Figure 6(d) shows the proton conductivity stability of the SPEEK/PDW-15 composite membrane immersed in liquid water at room temperature (25 °C). The proton conductivity stability of the SPEEK composite membrane with 15wt% unmodified HPW added (SPEEK/HPW-15) was also tested for comparison. The proton conductivity of the SPEEK/HPW-15 membrane decreased significantly within a short period due to the fact that the HPW in the SPEEK/HPW-15 membrane dissolved in water, resulting in the loss of HPW. In contrast, the proton conductivity of the SPEEK/PDW-15 membrane remained essentially unchanged over nearly three months, indicating that most of the PDW particles remain in the composite membrane. This phenomenon can be attributed to the amino groups on PDA bonding with HPW to form a stabilizing structure, which served to immobilize HPW.

To further investigate the proton transport mechanism in SPEEK/PDW composite membranes, the proton conductivity of the SPEEK control and SPEEK/PDW-15 composite membranes in liquid water at different temperatures was measured, and the corresponding Arrhenius plots of proton conductivity are shown in **Figure 7(a)**. Moreover, the activation energy (E_a) of proton transport in the membranes was calculated based on the Arrhenius plot [50]. The E_a values of the SPEEK control and SPEEK/PDW-15 membranes were 18.3 $kJ \cdot mol^{-1}$ and 15.8 $kJ \cdot mol^{-1}$, respectively, dropping in the range of 14–40 $kJ \cdot mol^{-1}$ [51]. This result indicated that the proton transport in the membranes was mainly dominated by the Grotthuss mechanism, where protons were transported by hydrogen bonding through jumps between proton conductors [51–53]. The E_a of the SPEEK/PDW-15 membrane was lower than that of the SPEEK control membrane. This suggested that doping PDW in the composite membranes reduced the potential barrier for proton transport and effectively shortened the proton hopping distance (**Figure 7(b)**).

The water uptake and proton conductivity of the SPEEK control and SPEEK/PDW-15 composite membranes at low RH are shown in **Figure 8(a)** and **Figure 8(b)**, respectively. The water uptake of the SPEEK/PDW-15 composite membrane was always higher than that of the SPEEK control membrane at the same RH (**Figure 8(a)**). This indicated that the water absorption capacity of PDW was stronger than that of SPEEK at low RH, which was mainly due to the excellent water

retention capacity of the HPW component in PDW. The proton exchange membrane was more favorable for proton transport at low RH when it had a stronger water retention capacity and more water. According to **Figure 8(b)**, the proton conductivity of the SPEEK/PDW-15 composite membrane decreased much slower than that of the SPEEK control membrane as RH decreased, especially when the RH was lower than 60%. The proton conductivity of the SPEEK/PDW-15 membrane was about an order of magnitude higher than that of SPEEK when the RH was below 45%. In addition to the higher water uptake of the composite membrane, the Keggin structure and the stronger acidity of HPW in PDW also played positive roles in proton transport.

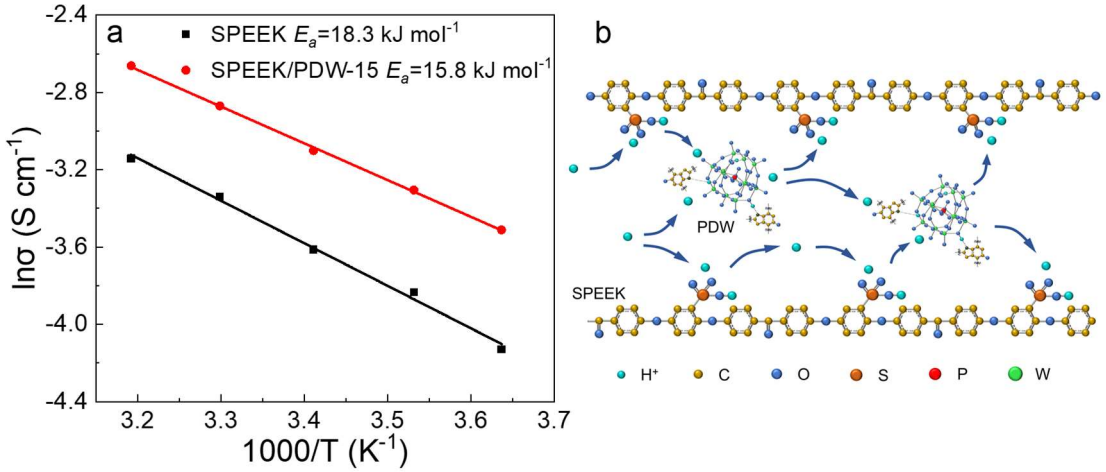

Figure 7. (a) Arrhenius plots of proton conductivity as function of temperature for SPEEK control and SPEEK/PDW-15 composite membranes. **(b)** Proposed mechanism for proton conduction in SPEEK/PDW composite membrane.

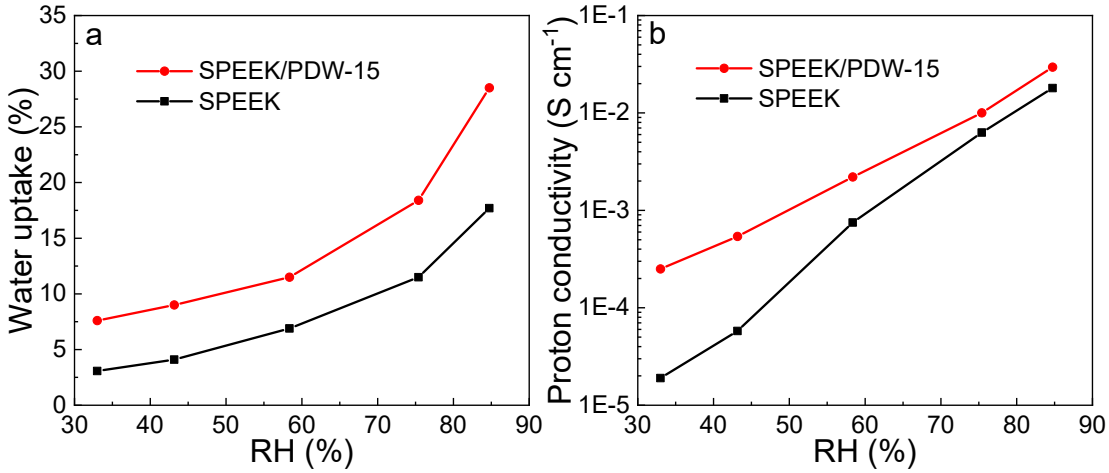

Figure 8. (a) Water uptake and **(b)** proton conductivity of SPEEK control and SPEEK/PDW-15 composite membranes under various RHs at 25 °C.

Figure 9 illustrates the stress-strain curves of the SPEEK control and SPEEK/PDW composite membranes. The tensile strength and elongation at the break of the SPEEK control membrane were 49.9 MPa and 101%, respectively. For the SPEEK/PDW composite membranes, both their tensile strength and elongation at the break were higher than those of the SPEEK control membrane when the loading of PDW was below 15 wt%. The tensile strength of the SPEEK/PDW-5 membrane was

the highest (59.6 MPa), which was considerably higher than that of the commercial Nafion 212 membrane (16.1 MPa) [54]. The elongation at the break of the SPEEK/PDW-15 membrane was the largest at 112%. The enhancement of the mechanical strength and toughness of the composite membranes can be attributed to the interactions generated between PDW and the SPEEK matrix, including acid-base interactions and hydrogen bonding [55,56]. When the filler content reached 20 wt%, the tensile strength of the composite membrane decreased due to the severe aggregation of the PDW hybrid.

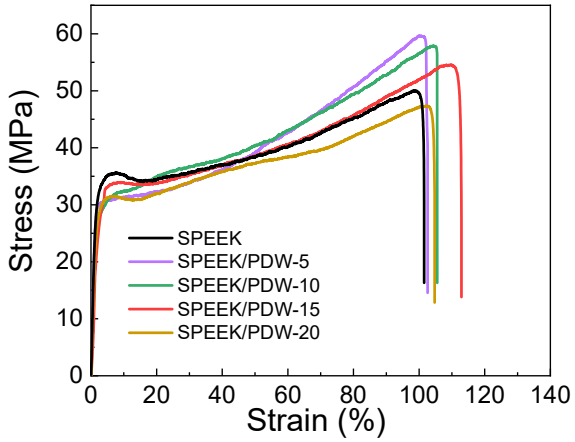

Figure 9. Stress-strain curves of SPEEK control and SPEEK/PDW composite membranes.

4. Conclusion

This work described the preparation of a water-insoluble PDW hybrid by the hydrothermal treatment of HPW and PDA. The XRD, FTIR, and XPS characterization results showed that HPW and PDA in PDW chemically bonded upon hydrothermal treatment, which resulted in the water-insolubility of PDW. The SEM analyses demonstrated that the SPEEK/PDW composite membranes exhibited excellent compatibility due to the strong interaction between sulfonic acid groups in the SPEEK matrix and PDW. This interaction also enabled the SPEEK/PDW composite membranes to maintain essentially unchanged area swelling in the presence of increased water uptake. The SPEEK/PDW-15 membrane achieved the highest proton conductivity of 0.052 $S \cdot cm^{-1}$, which was 63% higher than that of the SPEEK control membrane. The proton conductivity of the SPEEK/PDW-15 membrane was about an order of magnitude higher than that of SPEEK when RH was lower than 45%. Moreover, the proton conductivity of the SPEEK/PDW-15 composite membrane remained almost unchanged during the 80-day water immersion test. Thus, the present work provides a facile and promising method to prepare water-insoluble solid proton conductors for high-performance composite proton exchange membranes, which could be potentially applied to the fabrication of PEMFCs operating at high temperatures and low RH.

Author contributions: Data curation, ZL, XJ and XY; Conceptualization, JL and SH; methodology, JL and XJ; investigation, ZL, XJ and XY; writing—original draft

preparation, ZL; writing—review and editing, SH; visualization, ZL and SH; supervision, JL and SH; project administration, JL and SH; funding acquisition, JL and SH. All authors have read and agreed to the published version of the manuscript.

Acknowledgments: This work was supported by the National Natural Science Foundation of China (grant number: 51773058).

Conflict of interest: The authors declare no conflict of interest.

References

1. Yang W, Zhang E, Zhao J, et al. Dawn of clean energy: Enhanced heat transfer, radiative cooling, and firecracker-style controlled nuclear fusion power generation system. Clean Energy Science and Technology 2023; 1(1): 61. doi: 10.18686/cest.v1i1.61
2. Lu G, Wang Z, Bhatti UH, et al. Recent progress in carbon dioxide capture technologies: A review. Clean Energy Science and Technology 2023; 1(1): 32. doi: 10.18686/cest.v1i1.32
3. Zheng J, Chen X, Ma J. Advances in solid adsorbent materials for direct air capture of CO_2. Clean Energy Science and Technology 2023; 1(2): 95. doi: 10.18686/cest.v1i2.95
4. Chen J, Zhang W, Yang W, et al. Separation of benzene and toluene associated with vapochromic behaviors by hybrid 4 arene-based co-crystals. Nature Communications 2024; 15(1): 1260. doi: 10.1038/s41467-024-45592-6
5. Yan M, Wang Y, Chen J, et al. Potential of nonporous adaptive crystals for hydrocarbon separation. Chemical Society Reviews 2023; 52(17): 6075-6119. doi: 10.1039/d2cs00856d
6. Zhang R, Zhou J. Ultrafast-adsorption-kinetics molecular sieving of propylene from propane. Clean Energy Science and Technology 2024; 2(2): 126. doi: 10.18686/cest.v2i2.126
7. Harun NAM, Shaari N, Nik Zaiman NFH. A review of alternative polymer electrolyte membrane for fuel cell application based on sulfonated poly(ether ether ketone). International Journal of Energy Research 2021; 45(14): 19671-19708. doi: 10.1002/er.7048
8. Nimir W, AlOthman A, Tawalbeh M, et al. Approaches towards the development of heteropolyacid-based high temperature membranes for PEM fuel cells. International Journal of Hydrogen Energy 2023; 48(17): 6638-6656. doi: 10.1016/j.ijhydene.2021.11.174
9. Geiling J, Steinberger M, Ortner F, et al. Combined dynamic operation of PEM fuel cell and continuous dehydrogenation of perhydro-dibenzyltoluene. International Journal of Hydrogen Energy 2021; 46(72): 35662-35677. doi: 10.1016/j.ijhydene.2021.08.034
10. Kim AR, Poudel MB, Chu JY, et al. Advanced performance and ultra-high, long-term durability of acid-base blended membranes over 900 hours containing sulfonated PEEK and quaternized poly(arylene ether sulfone) in H_2/O_2 fuel cells. Composites Part B-Engineering 2023; 254: 110558. doi: 10.1016/j.compositesb.2023.110558
11. Rauf M, Wang JW, Zhang P, et al. Non-precious nanostructured materials by electrospinning and their applications for oxygen reduction in polymer electrolyte membrane fuel cells. Journal of Power Sources 2018; 408: 17-27. doi: 10.1016/j.jpowsour.2018.10.074
12. Elwan HA, Mamlouk M, Scott K. A review of proton exchange membranes based on protic ionic liquid/polymer blends for polymer electrolyte membrane fuel cells. Journal of Power Sources 2021; 484: 229197. doi: 10.1016/j.jpowsour.2020.229197
13. Kim AR, Vinothkannan M, Song MH, et al. Amine functionalized carbon nanotube (ACNT) filled in sulfonated poly (ether ether ketone) membrane: Effects of ACNT in improving polymer electrolyte fuel cell performance under reduced relative humidity. Composites Part B-Engineering 2020; 188: 107890. doi: 10.1016/j.compositesb.2020.107890
14. He S, Ai Y, Dai W, et al. Composite membranes anchoring phosphotungstic acid by β-cyclodextrins modified halloysite nanotubes. Polymer Testing 2021; 100: 107246. doi: 10.1016/j.polymertesting.2021.107246
15. Liu X, Li Y, Xue J, et al. Magnetic field alignment of stable proton-conducting channels in an electrolyte membrane. Nature Communications 2019; 10(1): 842. doi: 10.1038/s41467-019-08622-2
16. Liu X, Zhang J, Zheng C, et al. Oriented proton-conductive nano-sponge-facilitated polymer electrolyte membranes. Energy & Environmental Science 2020; 13(1): 297-309. doi: 10.1039/c9ee03301g

17. He S, Liu S, Dai W, et al. Nanocomposite Proton Exchange Membranes Incorporating Phosphotungstic Acid Anchored on Imidazole-Functionalized Halloysite Nanotubes. Journal of the Electrochemical Society 2018; 165(11): F951-F958. doi: 10.1149/2.0601811jes
18. Xu D, Zhang G, Zhang N, et al. Surface modification of heteropoly acid/SPEEK membranes by polypyrrole with a sandwich structure for direct methanol fuel cells. Journal of Materials Chemistry 2010; 20(41): 9239-9245. doi: 10.1039/c0jm02167a
19. Lee H, Dellatore SM, Miller WM, et al. Mussel-inspired surface chemistry for multifunctional coatings. Science 2007; 318(5849): 426-430. doi: 10.1126/science.1147241
20. Alfieri ML, Weil T, Ng DYW, et al. Polydopamine at biological interfaces. Advances in Colloid and Interface Science 2022; 305102689. doi: 10.1016/j.cis.2022.102689
21. Liu T, Kim KC, Lee B, et al. Self-polymerized dopamine as an organic cathode for Li- and Na-ion batteries. Energy & Environmental Science 2017; 10(1): 205-215. doi: 10.1039/c6ee02641a
22. Zhang C, Ou Y, Lei WX, et al. $CuSO_4/H_2O_2$-Induced Rapid Deposition of Polydopamine Coatings with High Uniformity and Enhanced Stability. Angewandte Chemie-International Edition 2016; 55(9): 3054-3057. doi: 10.1002/anie.201510724
23. Qi X, Huang Y, You S, et al. Engineering Robust Ag-Decorated Polydopamine Nano-Photothermal Platforms to Combat Bacterial Infection and Prompt Wound Healing. Advanced Science 2022; 9(11): 2106015. doi: 10.1002/advs.202106015
24. Wang Z, Zou Y, Li Y, et al. Metal-Containing Polydopamine Nanomaterials: Catalysis, Energy, and Theranostics. Small 2020; 16(18): 1907042. doi: 10.1002/smll.201907042
25. Liu Y, Ai K, Lu L. Polydopamine and Its Derivative Materials: Synthesis and Promising Applications in Energy, Environmental, and Biomedical Fields. Chemical Reviews 2014; 114(9): 5057-5115. doi: 10.1021/cr400407a
26. He S, Dai W, Zhai S, et al. Sulfonated poly(ether ether ketone) composite membranes based on amino-modified halloysite nanotubes that effectively immobilize phosphotungstic acid. Journal of Polymer Science 2020; 58(18): 2625-2633. doi: 10.1002/pol.20200035
27. Zhang Y, Wang H, Qian P, et al. Hybrid proton exchange membrane of sulfonated poly(ether ether ketone) containing polydopamine-coated carbon nanotubes loaded phosphotungstic acid for vanadium redox flow battery. Journal of Membrane Science 2021; 625: 119159. doi: 10.1016/j.memsci.2021.119159
28. Wei P, Huang D, Sui Y, et al. Polydopamine-coated polyimide nanofiber to anchor HPW and construct the pocket-like composite membrane with excellent proton conductivity and stability. International Journal of Hydrogen Energy 2023; 48(89): 34804-34815. doi: 10.1016/j.ijhydene.2023.05.284
29. Gong C, Liu H, Zhang B, et al. High level of solid superacid coated poly(vinylidene fluoride) electrospun nanofiber composite polymer electrolyte membranes. Journal of Membrane Science 2017; 535: 113-121. doi: 10.1016/j.memsci.2017.04.037
30. He S, Dai W, Yang W, et al. Nanocomposite proton exchange membranes based on phosphotungstic acid immobilized by polydopamine-coated halloysite nanotubes. Polymer Testing 2019; 73: 242-249. doi: 10.1016/j.polymertesting.2018.11.038
31. Zhai S, Lu Z, Ai Y, et al. High performance nanocomposite proton exchange membranes based on the nanohybrids formed by chemically bonding phosphotungstic acid with covalent organic frameworks. Journal of Power Sources 2023; 554: 232332. doi: 10.1016/j.jpowsour.2022.232332
32. Zhang Z, Ren J, Xu J, et al. Long-term durable solid state electrolyte membranes based on a metal-organic framework with phosphotungstic acid confined in the mesoporous cages. International Journal of Hydrogen Energy 2020; 45(51): 27527-27538. doi: 10.1016/j.ijhydene.2020.07.024
33. Feng M, Yu S, Wu P, et al. Rapid, high-efficient and selective removal of cationic dyes from wastewater using hollow polydopamine microcapsules: Isotherm, kinetics, thermodynamics and mechanism. Applied Surface Science 2021; 542: 148633. doi: 10.1016/j.apsusc.2020.148633
34. Elanthamilan E, Ganeshkumar A, Wang SF, et al. Fabrication of polydopamine/polyaniline decorated multiwalled carbon nanotube composite as multifunctional electrode material for supercapacitor applications. Synthetic Metals 2023; 298: 117423. doi: 10.1016/j.synthmet.2023.117423
35. Subudhi S, Mansingh S, Swain G, et al. HPW-Anchored UiO-66 Metal-Organic Framework: A Promising Photocatalyst Effective toward Tetracycline Hydrochloride Degradation and H_2 Evolution via Z-Scheme Charge Dynamics. Inorganic Chemistry 2019; 58(8): 4921-4934. doi: 10.1021/acs.inorgchem.8b03544

36. Zhang Z, Ren J, Xu J, et al. Enhanced proton conductivity of sulfonated poly(arylene ether ketone sulfone) polymers by incorporating phosphotungstic acid-ionic-liquid-functionalized metal-organic framework. Journal of Membrane Science 2021; 630: 119304. doi: 10.1016/j.memsci.2021.119304
37. Ma Y, Li A, Wang C, et al. Preparation of HPW@UiO-66 catalyst with defects and its application in oxidative desulfurization. Chemical Engineering Journal 2021; 404: 127062. doi: 10.1016/j.cej.2020.127062
38. Zhang J, He X, Yu S, et al. A novel dental adhesive containing Ag/polydopamine-modified HA fillers with both antibacterial and mineralization properties. Journal of Dentistry 2021; 111: 103710. doi: 10.1016/j.jdent.2021.103710
39. Zeng R, Deng H, Xiao Y, et al. Cross-linked graphene/carbon nanotube networks with polydopamine "glue" for flexible supercapacitors. Composites Communications 2018; 10: 73-80. doi: 10.1016/j.coco.2018.07.002
40. Huang X, Liu X. Morphology control of highly efficient visible-light driven carbon-doped POM photocatalysts. Applied Surface Science 2020; 505: 144527. doi: 10.1016/j.apsusc.2019.144527
41. Zhai S, Song H, Jia X, et al. Fabrication of water-insoluble phosphotungstic acid-carbon nitride nanohybrids for promoting proton transport of nanocomposite proton exchange membranes. Journal of Power Sources 2021; 506: 230195. doi: 10.1016/j.jpowsour.2021.230195
42. Kim JS, Choi MC, Jeong KM, et al. Enhanced interaction in the polyimide/sepiolite hybrid films via acid activating and polydopamine coating of sepiolite. Polymers for Advanced Technologies 2018; 29(5): 1404-1413. doi: 10.1002/pat.4252
43. Zhang X, Ma H, Pei T, et al. Anchoring HPW by amino-modified MIL-101(Cr) to improve the properties of SPEEK in proton exchange membranes. Journal of Applied Polymer Science 2023; 140(25): 53978. doi: 10.1002/app.53978
44. Dong C, Shi Z, Zhou Q. Preparation and investigation of acid-base composite membranes with modified graphitic carbon nanosheets for direct methanol fuel cells. Journal of Applied Polymer Science 2020; 137(45): 49388. doi: 10.1002/app.49388
45. Wang X, Rong Y, Wang F, et al. High performance proton exchange membranes with double proton conduction pathways by introducing MOF impregnated with protic ionic liquid into SPEEK. Microporous and Mesoporous Materials 2022; 346: 112314. doi: 10.1016/j.micromeso.2022.112314
46. Tsen W. Attapulgite solvent-free nanofluids modified SPEEK proton exchange membranes for direct methanol fuel cells. Ionics 2020; 26(11): 5651-5660. doi: 10.1007/s11581-020-03680-9
47. Zhong F, Zeng Z, Liu Y, et al. Modification of sulfonated poly (etherether ketone) composite polymer electrolyte membranes with 2D molybdenum disulfide nanosheet-coated carbon nanotubes for direct methanol fuel cell application. Polymer 2022; 249: 124839. doi: 10.1016/j.polymer.2022.124839
48. Murmu R, Roy D, Patra SC, et al. Preparation and characterization of the SPEEK/PVA/Silica hybrid membrane for direct methanol fuel cell (DMFC). Polymer Bulletin 2022; 79(4): 2061-2087. doi: 10.1007/s00289-021-03602-3
49. Zhu B, Sui Y, Wei P, et al. NH_2-UiO-66 coated fibers to balance the excellent proton conduction efficiency and significant dimensional stability of proton exchange membrane. Journal of Membrane Science 2021; 628: 119214. doi: 10.1016/j.memsci.2021.119214
50. Zhang Y, Wang H, Yu W, et al. Sulfonated poly(ether ether ketone)-based hybrid membranes containing polydopamine-decorated multiwalled carbon nanotubes with acid-base pairs for all vanadium redox flow battery. Journal of Membrane Science 2018; 564: 916-925. doi: 10.1016/j.memsci.2018.07.065
51. Zhai S, Jia X, Lu Z, et al. Highly ion selective composite proton exchange membranes for vanadium redox flow batteries by the incorporation of UiO-66-NH_2 threaded with ion conducting polymers. Journal of Membrane Science 2022; 662: 121003. doi: 10.1016/j.memsci.2022.121003
52. Zhai S, Lu Z, Ai Y, et al. Highly selective proton exchange membranes for vanadium redox flow batteries enabled by the incorporation of water-insoluble phosphotungstic acid-metal organic framework nanohybrids. Journal of Membrane Science 2022; 645: 120214. doi: 10.1016/j.memsci.2021.120214
53. Bano S, Negi YS, Illathvalappil R, et al. Studies on nano composites of SPEEK/ethylene glycol/cellulose nanocrystals as promising proton exchange membranes. Electrochimica Acta 2019; 293: 260-272. doi: 10.1016/j.electacta.2018.10.029
54. Wu J, Wang F, Fan X, et al. Phosphoric acid-doped Gemini quaternary ammonium-grafted SPEEK membranes with superhigh proton conductivity and mechanical strength for direct methanol fuel cells. Journal of Membrane Science 2023; 672: 121431. doi: 10.1016/j.memsci.2023.121431
55. Zhang Z, Liu H, Dong T, et al. Phosphonate poly(vinylbenzyl chloride)-Modified Sulfonated poly(aryl ether nitrile) for Blend Proton Exchange Membranes: Enhanced Mechanical and Electrochemical Properties. Polymers 2023; 15(15): 3203. doi: 10.3390/polym15153203

56. Xiao Y, Shen X, Sun R, et al. Polybenzimidazole membrane crosslinked with quaternized polyaniline as high-temperature proton exchange membrane: Enhanced proton conductivity and stability. Journal of Membrane Science 2022; 660: 120795. doi: 10.1016/j.memsci.2022.120795